Interface Structure in Nb_2O_5/Al Nanocomposites Processed by High-Pressure Torsion at Room Temperature

Clênio Silva[1], Luciano A. Montoro[2], Débora A. A. Martins[2], Priscila A. Machado[1], Pedro Henrique R. Pereira[1], Berenice M. Gonzalez[1], Terence G. Langdon[3], Roberto B. Figueiredo[1], Augusta Isaac[1,*]

[1] Department of Metallurgical and Materials Engineering, Universidade Federal de Minas Gerais, Belo Horizonte, MG 31270-901, Brazil.

[2] Department of Chemistry, Universidade Federal de Minas Gerais, Belo Horizonte, MG 31270-901, Brazil.

[3] Materials Research Group, Department of Mechanical Engineering, University of Southampton, Southampton SO17 1BJ, UK.

Abstract. Extremely thin Nb_2O_5 nanowires and Al powder were successfully consolidated at room temperature by using high-pressure torsion (HPT), producing a novel metal matrix nanocomposite with exceptional mechanical properties. It is shown that minor additions of Nb_2O_5 increase sharply the hardness of commercially pure Al. For instance, hardness of over 180 Hv was developed at the edge of samples with 10% nanowires and processed through 10 turns of HPT. This is markedly higher than any other value reported for pure aluminum matrix composites having this level of reinforcement phase. A detailed characterization of the interface structure using high-angle annular dark field scanning transmission electron microscopy (HAADF-STEM) revealed a pronounced grain refinement of the Al matrix at the nanoscale and the occurrence of the aluminothermic reduction of the Nb_2O_5. The latter led to: (i) the formation of Al_2O_3 nanolayer at the Al/Nb_2O_5 interface and (ii) the nanosegregation of metallic Nb (with few atomic layers) along grain boundaries and dislocations. The pronounced increase in hardness is attributed to the formation of this interface nanostructure.

Keywords: high-pressure torsion; nanocomposite; niobium oxide; segregation; hardness

***Corresponding author**: augusta.cerceau@demet.ufmg.br

1. INTRODUCTION

In pursuit of lightweight and high-performance materials for the aerospace and automotive sectors, aluminum-based composites have emerged as a promising class of materials for the replacement of conventional metallic alloys in many applications [1,2]. Metal-matrix nanocomposites (MMNCs) are particularly important and may be developed with properties that are superior to those of monolithic alloys and composites containing micron-scale reinforcements [2,3]. Ceramic nanoparticles, such as Al_2O_3, SiC, TiC, and AlN, are commonly used as reinforcements in Al-MMNCs. More recently, carbon nanotubes (CNTs) were investigated as a reinforcing phase in MMNCs because of their high aspect ratio, high elastic modulus (> 1 TPa) and high tensile strength (> 30 GPa) [4,5].

The processing technique employed in the synthesis of Al-based nanocomposites has a significant influence on their microstructural characteristics such as the dispersion of the reinforcing phase in the matrix and the nature of the reinforcement/matrix interface, and this in turn has direct implications for their mechanical properties. To date, Al-MMNCs have been produced by liquid, semi-solid and solid processing routes [6]. Liquid processing routes, in particular, are quite challenging due to the poor wettability of the reinforcing phase in a molten matrix and the large difference in density between the reinforcements and the metallic matrix. In addition, undesired interfacial reactions are likely to occur due to the high temperatures achieved during processing [6–8]. Although to a lesser extent than in liquid-state processing, the difficulty in obtaining a uniform distribution of reinforcements occurs also in matrices in the semi-solid state [6]. Considering the drawbacks associated with the production of Al-nanocomposites by liquid and semi-solid processing routes, solid-state processing is generally considered the most attractive alternative procedure.

Solid-state processing techniques for the production of MMNCs are generally based on powder metallurgy (PM) procedures. In practice, these processes usually involve the following steps: (i) a blending/mixing of the metal-matrix and reinforcement powder; (ii) compacting the blend usually by cold pressing (called “green compacts”); and (iii) a sintering of the green compacts through different routes such as direct sintering, microwave-assisted sintering [9], spark plasma sintering [10], hot extrusion [11] and severe plastic deformation (SPD) [12,13]. The major advantages of these PM techniques are the significant reduction in wettability-related problems, the possibility

of producing composite systems which are not feasible using the liquid or semi-solid processing routes, and a generally improved control of the chemical reactions involved during processing [6]. Further improvements in the mechanical performance of the MMNCs depends largely on producing a strong matrix-reinforcement interface which ,may be obtained through a high degree of coherency, mechanical bonding induced by surface roughness, appropriate reactions or through interdiffusion bonding[14,15].

Great progress has been achieved in the development of MMNCs by incorporating nanoparticles through SPD procedures, including by use of high-pressure torsion (HPT) which offers a possibility to consolidate metal-matrix composites with a simultaneous grain refinement which may be even to the nanometer level [16–18]. In the HPT process, a disk-shaped sample is placed between two anvils under a nominal pressure of 2 - 8 GPa and rotated in a quasi-constrained condition up to a chosen number of turns (N). The severe shear straining and high hydrostatic pressure makes the consolidation feasible even at room temperature (RT) [5,19–21]. Solid-state joining processes, such as mechanical alloying and chemical intermixing, often occur during the HPT processing leading to the consolidation of multicomponent materials at low homologous temperatures [20]. For example, ultrahigh-strength tungsten-based nanocomposites (W/Al, W/Ti, and W/Ni) with average grain sizes ranging from 9 to 15 nm were successfully produced by HPT at 573 K where this is a temperature at which the occurrence of detrimental interfacial reactions or the formation of brittle intermetallics can be prevented [22].

In addition to grain refinement, recent studies have shown that HPT-processed composites exhibit a ‘hierarchical interface structure’ which can dramatically affect the structure-property relationship of these materials [14,23,24]. The interface architecture of these materials encompasses multiple length scales compromising: (i) grain boundaries (GBs), (ii) interfaces between the matrix and reinforcing phase, (iii) subgrain boundaries and other types of interfaces at the nanometer scale; (iii) inter- and/or transgranular elemental segregation; and (iv) subnanometer intragrunular solute-clustering [14,23,24]. A fundamental understanding and control of these interface structures holds promise for developing the ability to tailor the mechanical behavior of new generations of these lightweight composite systems. Accordingly, the present research was initiated to investigate the interface structures and hardness evolution of

Al-based MMNCs reinforced with Nb_2O_5 nanowires fabricated by HPT at room temperature.

2. MATERIALS AND METHODS

The Nb_2O_5/Al nanocomposites were produced by HPT at room temperature. Spherical Al powders with a purity of 99.7% and an average particle size of ~9 μm were used as metallic matrices in the nanocomposites. The Nb_2O_5 nanowires were synthesized using a solvothermal method. Ammonium niobate oxalate hydrate ($NH_4[NbO(C_2O_4)_2(H_2O)_2]\cdot 3H_2O$) was processed by a solvothermal method in a microwave reactor using alcohol as a solvent upon heating for 30 minutes. The resulting material was filtered and washed with acetone. This synthesis procedure is a patent pending method/material and a detailed description is now in preparation. The nanostructured material is constituted of high quality and homogenous bundles of aggregated thin nanowires of Nb_2O_5 in an orthorhombic crystal structure. Figure 1 shows scanning electron microscopy (SEM) and high-resolution transmission electron microscopy (HRTEM) images of these wires. The Nb_2O_5 nanowires were of several hundreds of nm in length and ~3 nm in diameter.

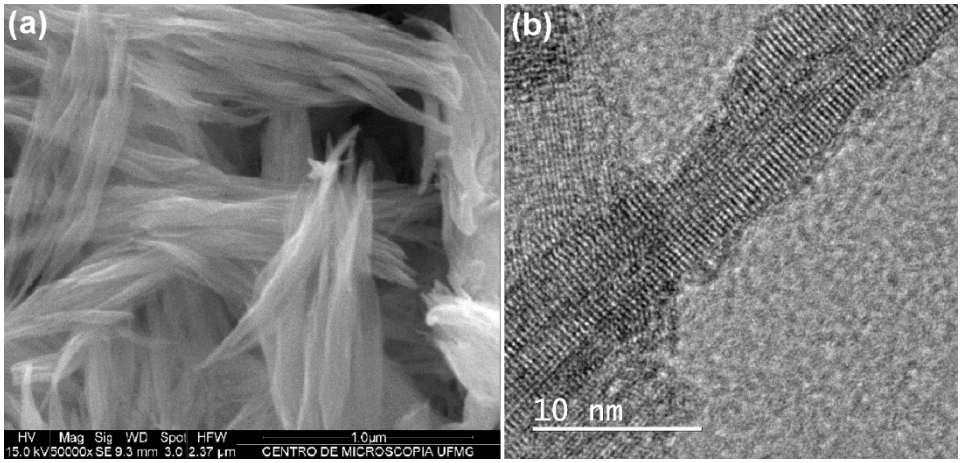

Figure 1. The Nb_2O_5 nanowires used as reinforcing phase in the Al- Nb_2O_5 nanocomposites. (a) SEM image of the bundles of aggregated thin nanowires of Nb_2O_5. (b) HRTEM image of a representative monocrystalline Nb_2O_5 nanowire, exhibiting approximately 3 nm in diameter.

Six distinct composites were produced using the Al powder reinforced with 0.5%, 1%, 2%, 3%, 5%, and 10% in weight of Nb_2O_5 nanowires. Firstly, Nb_2O_5 nanowires were blended with pure aluminum powder and mechanically homogenized using ball milling for 15 min. After homogenization, disks having diameters and thicknesses of 10.0 mm and 1.2 mm, respectively, were obtained by compacting the mixtures in a hydraulic press at RT. Thereafter, pre-compacted disks were processed by HPT at RT using a quasi-constrained facility [25] operating at a nominal pressure of 6.0 GPa and using a rotation rate of ~2 rpm. Samples were processed to 5 and 10 turns in order to track the evolution of the consolidation process. For comparison purposes, a disk of bulk pure aluminum was also processed by HPT.

The microstructures of the nanocomposites were characterized using high-resolution scanning transmission electron microscopy (STEM) imaging on a FEI Titan Themis Cubed (FEI Company), equipped with a Cs probe corrector and a Super-X EDS with four windowless silicon-drift detectors and operated at 300 kV. The STEM observation was performed at the half-radius position of the HPT-processed disks. Thin TEM lamellas were prepared using the dual-beam focused-ion-beam workstation Quanta FEG 3D FEI. Hardness measurements were performed on the consolidated samples, applying a load of 100 gf during 10 s in a Future-Tech FM-700 tester equipped with a Vickers diamond indenter. Measurements were performed along the diameter of the Nb_2O_5/Al nanocomposites with varying concentration of Nb_2O_5 (0.5%, 1%, 2%, 3%, 5%, and 10% in weight) after 5 and 10 turns. For comparison purposes, microhardness measurements were also performed on HPT-processed Al disks after 5 turns.

3. RESULTS

a. Mechanical response of the Nb_2O_5/Al nanocomposites

The effect of the addition of Nb_2O_5 nanowires into the pure Al matrix on the Vickers microhardness values is presented in Figure 2. The microhardness of the HPT-processed pure Al disks reached a saturation level of about 80 Hv after 5 HPT turns as shown by the lower datum points in Figure 2(a). A significant improvement in Vickers microhardness was achieved with the addition of the Nb_2O_5 nanowires into the Al matrix. The hardness profile of all MMNCs exhibited greater values at the edges of the disks which is attributed to the larger torsional strain in this region compared to the

center. The samples with only 0.5% and 1.0% of nanowires exhibit hardness values of ~120 Hv after only 5 turns of HPT and this is in the range of hardness observed in aluminum matrix composites having much higher fractions of the reinforcement phase. For example, hardness values in the range of ~80-120 Hv were reported in Al-3% CNT [19], Al-5% CNT [4], Al-5% fullerene [26], Al-5% graphene [27] and Al-10% Al_2O_3 [28] processed by HPT.

The composites reinforced with 5% and 10% wt. Nb_2O_5 exhibited hardness values over ~140 Hv after five HPT turns. Further processing to 10 turns promoted a slight increase in hardness of the composites with 0.5 – 5% of nanowires but the sample with 10% wt. of nanowires exhibited a significant increase in hardness to ~190 Hv after 10 turns at the edge of the disc. This is markedly higher than any other values reported for pure aluminum matrix composites having this level of reinforcement phase.

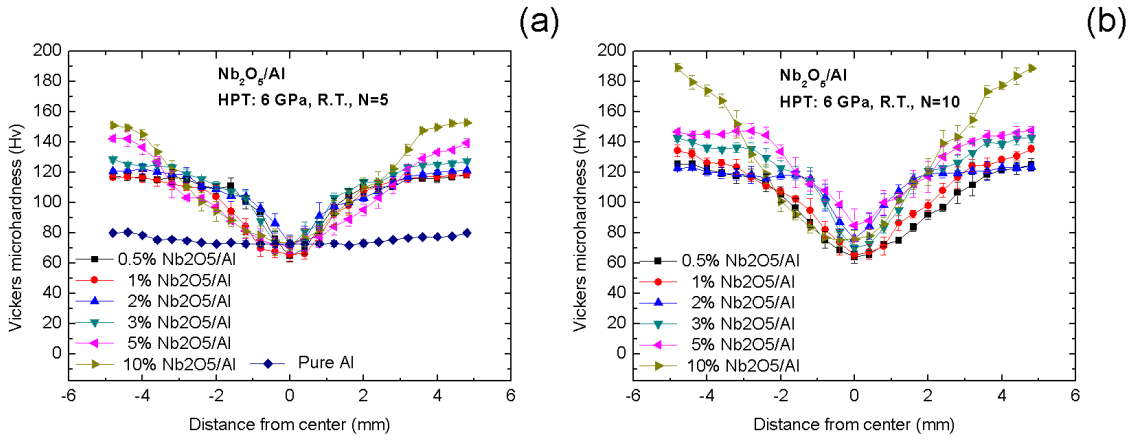

Figure 2. Microhardness profiles of the HPT-processed Nb_2O_5/Al nanocomposites with varying concentration of Nb_2O_5 (0.5%, 1%, 2%, 3%, 5%, and 10% in weight) after 5 (a) and 10 turns (b).

b. Microstructure of the Nb_2O_5/Al nanocomposites

To reveal the origins of these outstanding hardness values, the hierarchical interface structure of the HPT-processed 10% wt. Nb_2O_5/Al nanocomposites was investigated using aberration-corrected scanning transmission electron microscopy (STEM) equipped with both bright-field (BF) and high-angle annular dark-field (HAADF) detectors. HAADF-STEM provides high-resolution images where the

imaging contrast is related to the local atomic number (Z). [29–31]. As a result, sample regions with heavier elements tend to be brighter than regions with lighter elements such as oxygen or the light metals. The bright-field imaging is also related to a Z-contrast, but with an inverse contrast, where heavier components appear as dark regions and light components as bright regions. However, the BF imaging is also influenced significantly by diffraction effects where the image contrast must be analyzed by considering both effects: Z-contrast and diffraction. Figures 3 and 4 display typical BF and the corresponding HAADF-STEM images of the 10% wt. Nb_2O_5/Al nanocomposites after 5 and 10 HPT turns, respectively.

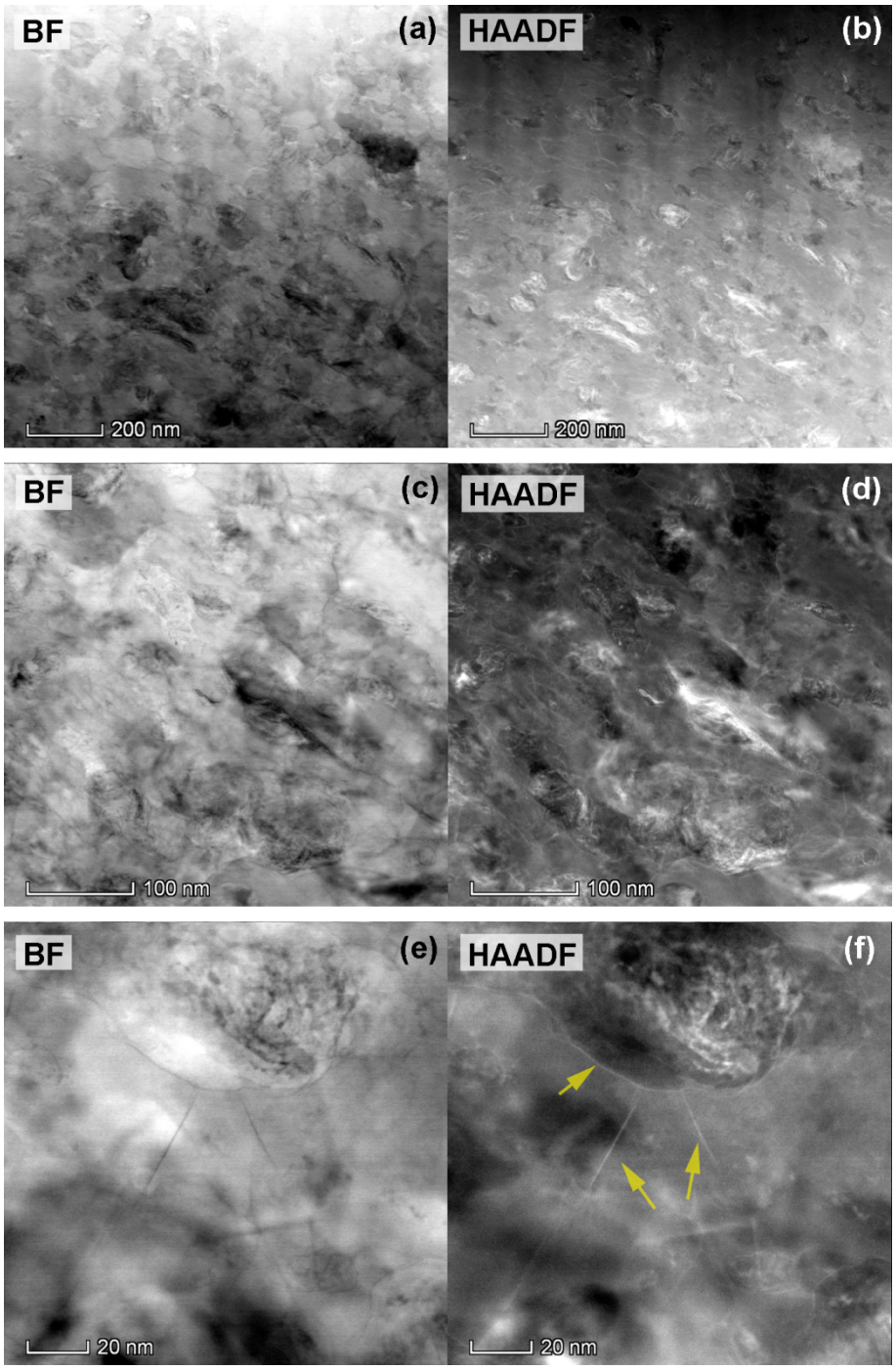

Figure 3. BF-STEM (left) and their corresponding HAADF-STEM images (right) of the 10% wt. Nb_2O_5/Al nanocomposites after 5 HPT turns. Evidence of segregation of heavy atoms to crystalline defects is indicated by yellow arrows.

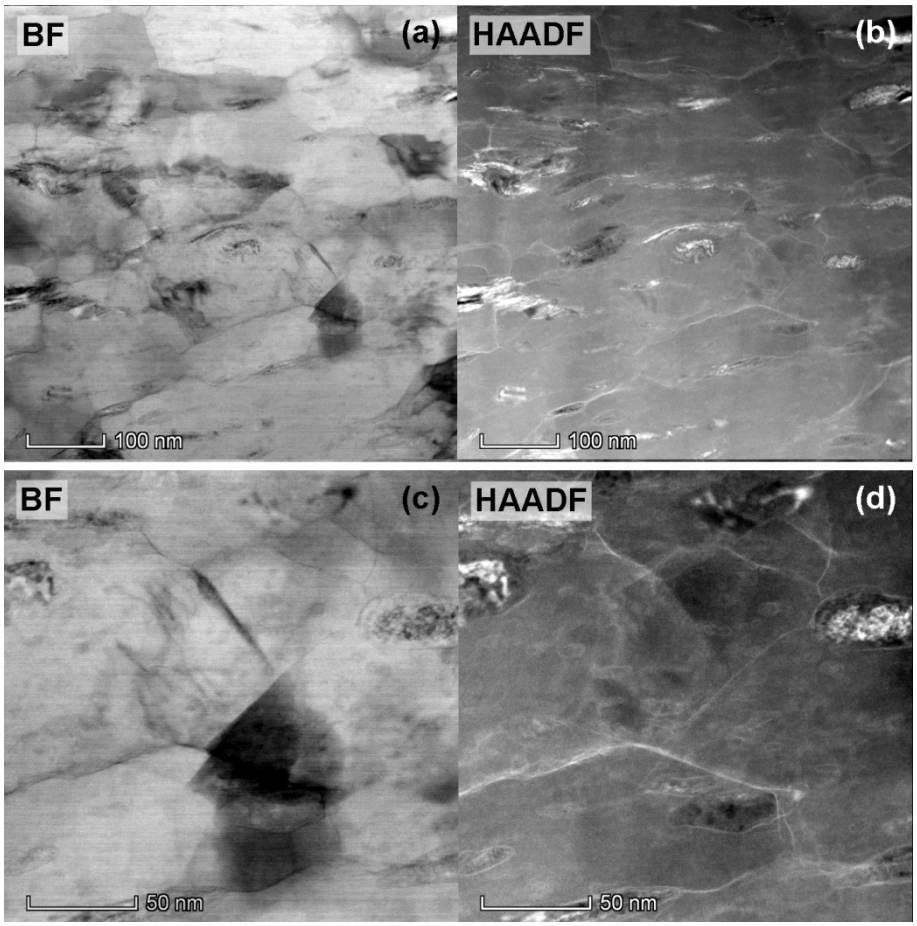

Figure 4. BF-STEM (left) and their corresponding HAADF-STEM images (right) of the 10% wt. Nb_2O_5/Al nanocomposites after 10 HPT turns.

The BF-STEM images of the 10% wt. Nb_2O_5/Al nanocomposite after 5 turns reveal slightly elongated grains of ~100 nm in length and ~60 nm in width (Figure 3(a)). An inhomogeneous diffraction contrast caused by the high density of dislocations is noted within the grains, especially near the agglomerations of Nb_2O_5 particles in Figure 3(a). After 10 HPT turns, the BF-STEM images in Figure 4(a) and 4(c) depict grains with approximately the same size as in the previous deformation state but with a considerable reduction in the dislocation density.

The HAADF-STEM images of the 10% wt. Nb_2O_5/Al nanocomposite show that the original morphology of the reinforcing phase, which were thin nanowires, changed to tangles of fragmented particles after 5 HPT turns, thereby forming clusters ranging from tens to hundreds of nanometers, as shown by the bright regions in Figure 3(b,d,f). Larger numbers of HPT turns led to a partial de-agglomeration of the reinforcements with a more uniform distribution in the Al matrix (Figure 4). Moreover, these images

provide evidence of segregation of heavy atoms to dislocations, grain boundaries (GBs) and subgrain boundaries, as indicated by the arrows in Figure 3.

Figure 5 depicts the STEM-EDS elemental mappings with the overall composition of the reinforcements and segregations formed in the 10% Nb_2O_5/Al nanocomposites after 10 HPT turns. These chemical maps confirm that Nb and O atoms are uniformly distributed in 50 – 70 nm aggregates of the reinforcement phase. A close-up inspection in Figure 5 reveals the presence of oxygen superimposed on aluminum, forming a layer of about a few nanometers thick at the Nb_2O_5/Al interface. These results suggest the formation of aluminum oxide as a result of the reduction of Nb_2O_5 during the HPT processing.

Figure 6 displays STEM and EDS elemental maps of the long and thin structures formed during the HPT processing. The elemental mappings demonstrate that these structures also consist of metallic niobium with no oxygen superimposed on the Nb signal. These results confirm the aluminothermic reduction of Nb_2O_5 through the reaction

$$3Nb_2O_5 + 10Al \rightarrow 6Nb + 5Al_2O_3.$$

The thickness of these structures is about 5 nm which is equivalent to approximately 15 atomic layers of niobium. The HAADF-STEM images shown in Figure 7(a and b), confirm that these structures can be attributed to metallic niobium. This high-resolution STEM pattern with 2.34 Å of lattice spacing is unequivocally indexed to the Nb (110) lattice planes. Figure 7(b) also indicates the formation of small Nb nanoparticles having sizes of less than ~2 nm. Furthermore, the HAADF- and BF-STEM images, shown in Figure 7(c and d), exhibit niobium segregation layers of ~1.5 nm thickness along subgrain boundaries. From Figure 7(d) it is observed that these defect-free aluminum subgrains are oriented at different crystallographic positions. The corresponding fast Fourier transform (FFT) pattern can be indexed to (200) and (111) aluminum lattice planes. This suggests that, despite the presence of a Nb layer, the Al subgrains are related by a crystallographic orientation along the [011] zone axis.

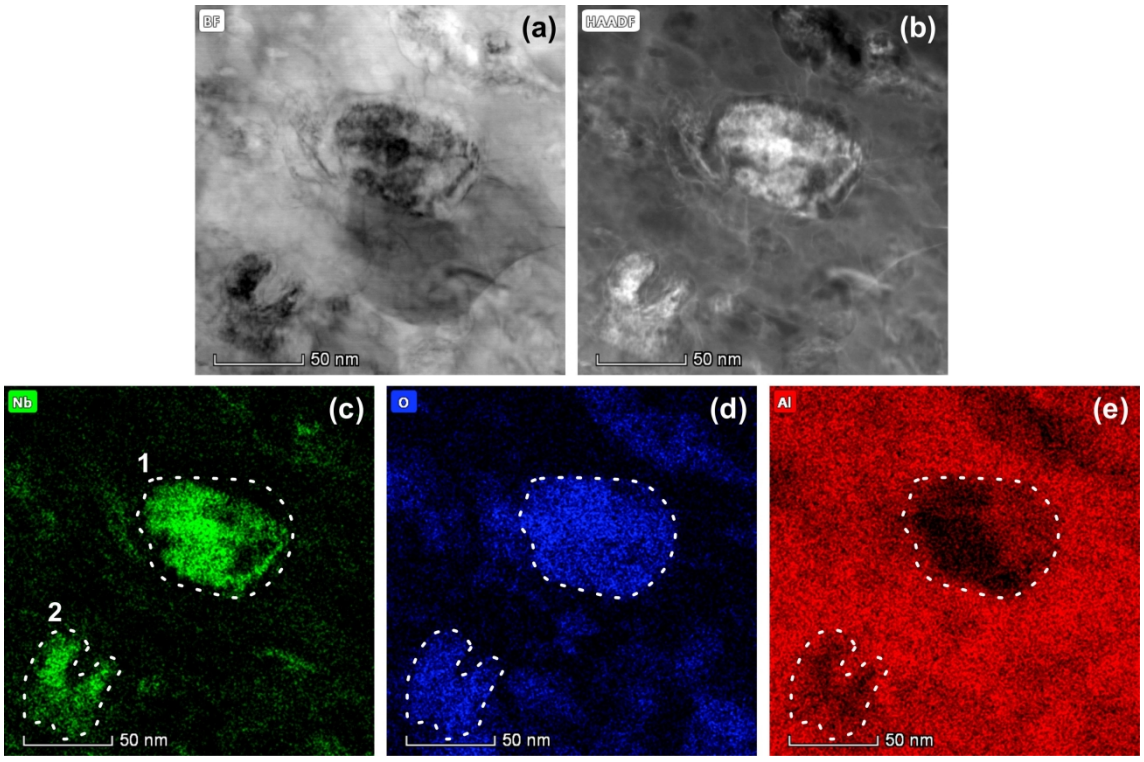

Figure 5. HAADF-STEM image and EDS elemental mappings of the Nb_2O_5 agglomerations formed in the 10% wt. Nb_2O_5/Al nanocomposites after 10 HPT turns, showing Al (red), Nb (green), and O (blue).

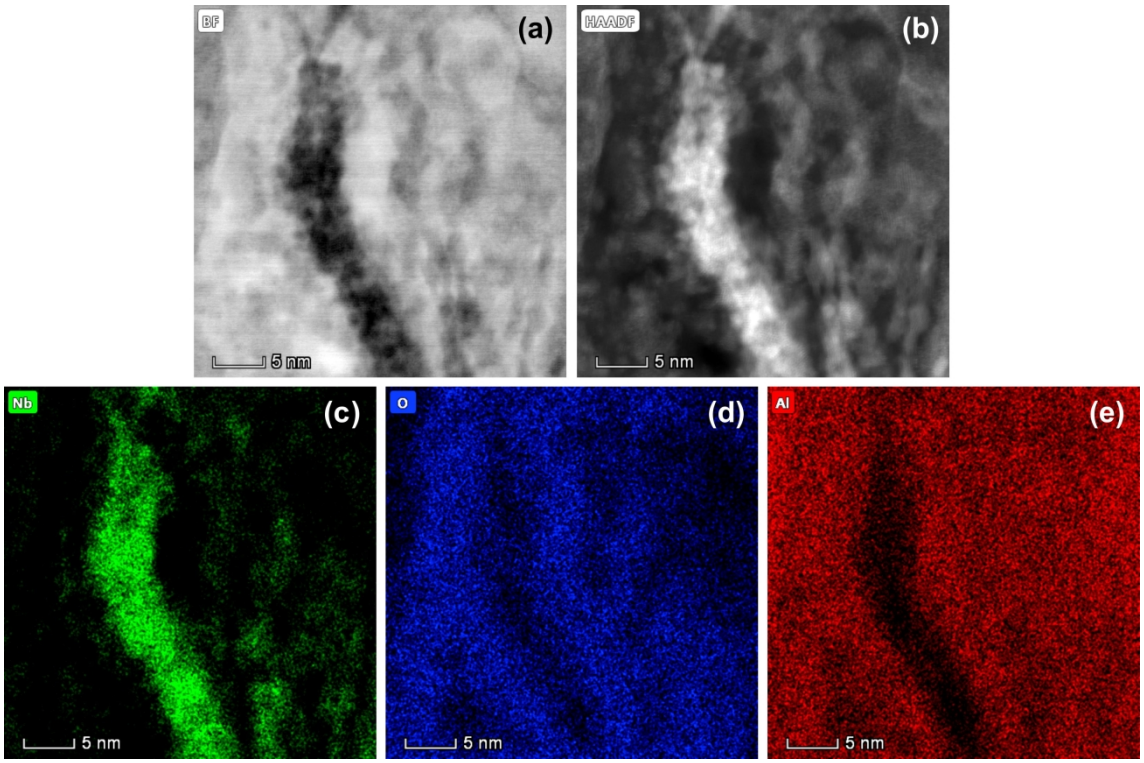

Figure 6. HAADF-STEM image and EDS elemental mappings revealing the segregation of Nb atoms along planar defects in the 10% wt. Nb_2O_5/Al nanocomposites after 5 HPT turns.

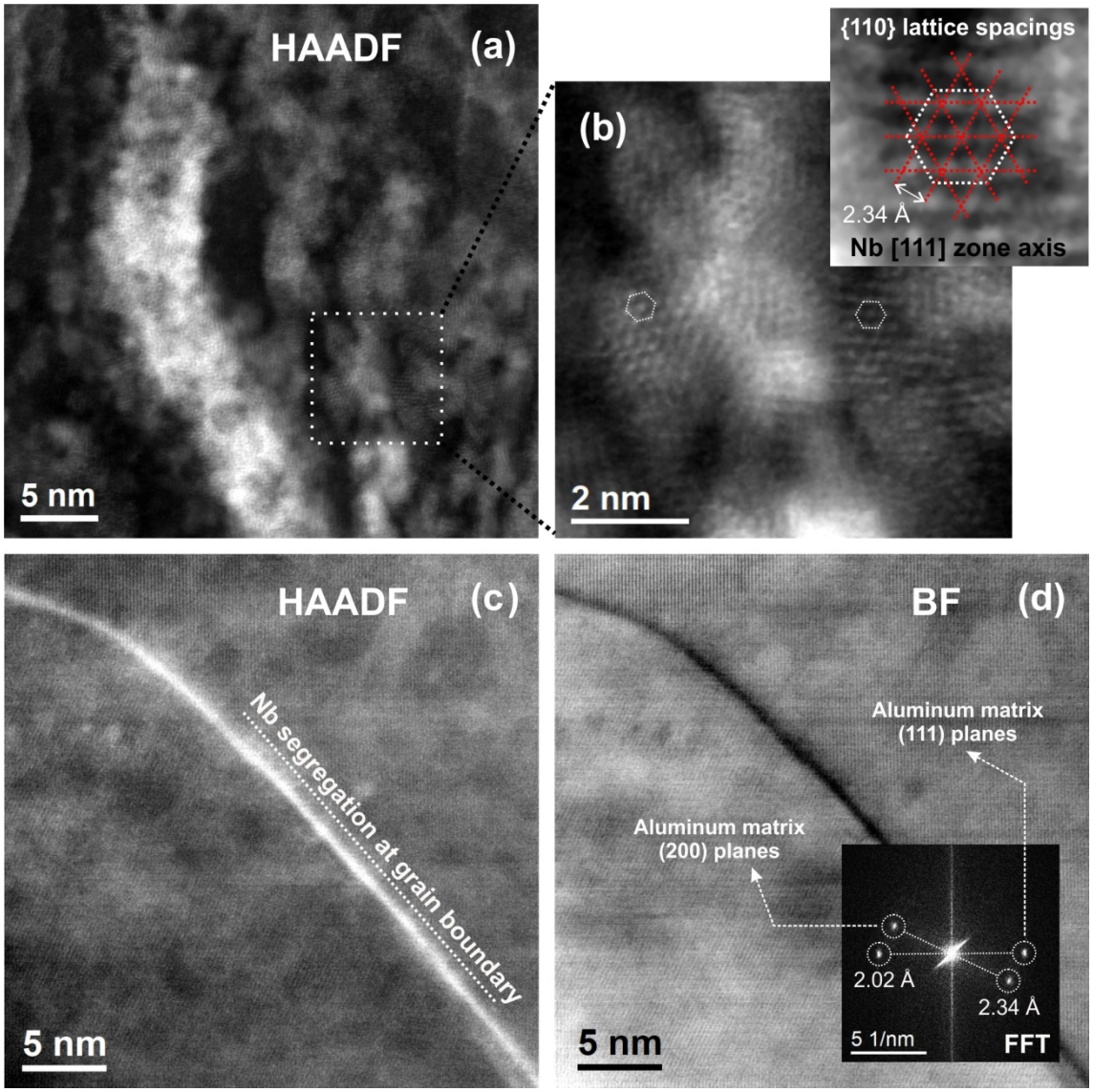

Figure 7. Microstructure of the 10% wt. Nb_2O_5/Al nanocomposites after 10 HPT turns. HAADF-STEM image exhibiting the nanometer-scale niobium segregation (a) and a zoomed image of the region marked in (a) and the corresponding FFT pattern (b). HAADF- and BF-STEM images (c and d, respectively) showing the niobium segregation along subgrain boundaries.

4. DISCUSSION

a. Aluminothermic reduction of Nb_2O_5 and the niobium segregation

The aluminothermic reduction of Nb_2O_5 followed by niobium segregation at linear and planar defects, to the detriment of intermetallic compound formation, may be examined in terms of thermodynamic and kinetic factors. Thermodynamically, pure Al

and Al_3Nb are the stable phases at room temperature in the Al-Nb system [32,33]. The enthalpy of formation of Al_3Nb at 298 K is ~121 kJ/mol [34] and the heat of reaction of the aluminothermic reduction of Nb_2O_5 is ~890 kJ/mol [35]. In high energy milling experiments of the Al and Nb_2O_5 powders for 45, 75, and 120 minutes at 298 K, X-ray diffraction of the milled mixtures detected the presence of Al_2O_3 and Nb as result of the aluminothermic reduction of niobium pentoxide only after 75 minutes [34]. The solid-state reaction was also reported in an Al-50%$_{at.}$ Ni composite during HPT, leading to the formation of an Al_3Ni_2/Ni nanocomposite [36].

Therefore, it is important to examine the reason for the lack of formation of Al_3Nb during HPT at room temperature. This can be explained by the diffusion kinetics in the Al-Nb system and the enhanced solubility limit in crystalline defects. The diffusion kinetics for the formation of Al_3Nb was studied from 800 to 1300 ^oC [36] and both the activation energy and the pre-exponential factor were estimated as ~152.7 kJ mol^{-1} and ~5.4 x 10^{-4} m^2 s^{-1}. By considering these parameters, the kinetic constant at room temperature (30^oC) is estimated to be in the order of ~10^{-30} while at 1000^oC it is ~10^{-10}. From these estimates, it is concluded that the formation of Al_3Nb at low temperatures requires a long time and there will be no formation of such phase during the few minutes associated with conventional HPT processing.

In addition, it was shown that solute segregation at linear and planar defects takes place during the HPT processing of aluminum alloys and the presence of Nb atoms in the Al matrix leads to a compressive strain with a strong tendency for segregation at defect sites in order to minimize the elastic strain [23]. The other factor influencing solute segregation is the potential for an increase of over 1 order of magnitude in the interdiffusion coefficients for severely deformed materials [37]. In SPD-processed materials, the high density of defects reduces the energy barrier for diffusion [37] and the high diffusion rates do not permit a local concentration of Nb and therefore they preclude the formation of Al_3Nb.

b. Hardening mechanisms

As shown in Figure 1, the hardness at the edge of the Al-10% wt. Nb_2O_5 disks after 10 HPT turns (~190 Hv) is very substantially higher than in both the HPT-processed pure Al disk (~80 Hv) and the nanocomposites with lower fractions of the reinforcement phase. The strengthening mechanisms contributing to these high hardness

values are mainly Hall-Petch strengthening, the Orowan mechanism, nanoscale segregation and any load-bearing effect.

First, the nanocrystalline grain size accounts for the alloy strength through restriction of dislocation mobility as described by the Hall–Petch relationship [38,39]. According to the Orowan mechanism, when a dislocation passes a reinforcement particle then a residual dislocation loop remains around the particle. This interaction between hard nanoparticles and dislocations may contribute significanly to the composite strength [40,41] but in practice it is reasonable to anticipate that this mechanism plays only a minor role in the present nanocomposites. Thus, the agglomeration of the reinforcement phase increases the mean distance between the Nb_2O_5 nanowires and in practice hard nanoparticles were not observed in the grain interiors so that the main barriers to dislocation movement are GBs and subgrain boundaries.

The present structural and chemical analyses of the Nb_2O_5/Al MMNCs using HAADF-STEM provides direct evidence for nanometer-sized structures consisting of Nb atoms at GBs, subgrains and other defects [42]. It is expected that the intergranular solute segregation provides a stabilization of grain growth [24] and a strengthening of the mechanical bonding at the interface [15], where the latter hinders the nucleation of dislocations at the GBs [24]. Earlier studies demonstrated that solute segregation causes an increase in the stress required to initiate grain boundary-mediated plastic deformation, sduch as grain boundary sliding and grain rotation, in nanocrystalline metals [43].

Strong interfacial bonding between the reinforcements and the matrix plays also a critical role in the mechanical response of the composites. The present STEM-EDS elemental mappings of the nanocomposites confirms there is an interfacial reaction between the Nb_2O_5 and the Al matrix during HPT processing. The aluminothermic reduction of Nb_2O_5 leads to the formation of an Al_2O_3 nanolayer at the Nb_2O_5/Al interface. Using high-resolution TEM, the Al/Al_2O_3 interface was observed to match the close-packed planes and directions in the two phases [44,45]. Therefore, the modification of the interface from Nb_2O_5/Al to Nb_2O_5/Al_2O_3/Al appears to lead to an enhanced interfacial bonding and thus to an effective load transfer from the Al matrix to Nb_2O_5 and Al_2O_3. It should be noted also that alumina whiskers were recently in-situ synthesized in CNT-reinforced aluminum nanocomposites [46] and it was reported that

the Al_2O_3 layer formed on the outer-walls of the CNTs provide a strong interfacial bonding which effectively promotes a load transfer from the Al matrix to the carbon nanotubes [46,47]. It is proposed that an analogous type of behavior, associated with enhanced interfacial bounding, accounts also for the high hardness values recorded around the periphery of the Al-10% wt. Nb_2O_5 disks after HPT though 10 turns.

5. SUMMARY AND CONCLUSIONS

1- Niobium pentoxide nanowires were synthesized in the laboratory and incorporated at different fractions into a pure aluminum matrix using room temperature consolidation of powders by high-pressure torsion.

2- The hardness of the composites increased significantly with only 0.5% wt. of nanowires and there was an exceptionally high increase in hardness with 10% wt. of nanowires after 10 turns of HPT.

3- HAADF-STEM images revealed a solid-state reaction during HPT. An aluminothermic reduction of Nb_2O_5 was observed along a thin layer of nanowire agglomerates leading to the formation of Al_2O_3 and Nb. These Nb atoms segregated at crystal defects.

4- The segregation of Nb at grain boundaries restricts grain growth leading to the formation of nanostructured grains and contributes directly to the high hardness of the composite.

6. ACKNOWLEDGEMENTS

The authors acknowledge LME/LNNano/CNPEM for providing the equipment and technical support during the experiments involving electron microscopy. AI acknowledges the financial support from FAPEMIG (grant # APQ-02786-14); and RBF, CNPq (grant #400407/2016-7) and FAPEMIG (grant #APQ-00580-15). TGL was supported in part by the European Research Council under ERC Grant Agreement No. 267464-SPDMETALS.

7. DATA AVAILABILITY

The raw/processed data required to reproduce these findings cannot be shared at this time due to technical or time limitations

8. REFERENCES

[1] D.K. Koli, G. Agnihotri, R. Purohit, Advanced Aluminium Matrix Composites: The Critical Need of Automotive and Aerospace Engineering Fields, in: Mater. Today Proc., 2015: pp. 3032–3041. doi:10.1016/j.matpr.2015.07.290.

[2] F. Chen, N. Gupta, R.K. Behera, P.K. Rohatgi, Graphene-Reinforced Aluminum Matrix Composites: A Review of Synthesis Methods and Properties, JOM. 70 (2018) 837–845. doi:10.1007/s11837-018-2810-7.

[3] J. Zhou, L. Ren, X. Geng, L. Fang, H. Hu, As-cast magnesium AM60-based hybrid nanocomposite containing alumina fibres and nanoparticles: Microstructure and tensile behavior, Mater. Sci. Eng. A. 740–741 (2019) 305–314. doi:10.1016/j.msea.2017.10.070.

[4] T. Tokunaga, K. Kaneko, Z. Horita, Production of aluminum-matrix carbon nanotube composite using high pressure torsion, Mater. Sci. Eng. A. 490 (2008) 300–304. doi:10.1016/j.msea.2008.02.022.

[5] K. Aristizabal, A. Katzensteiner, A. Bachmaier, F. Mücklich, S. Suárez, On the reinforcement homogenization in CNT/metal matrix composites during severe plastic deformation, Mater. Charact. 136 (2018) 375–381. doi:10.1016/j.matchar.2018.01.007.

[6] L. Ceschini, A. Dahle, M. Gupta, A.E.W. Jarfors, S. Jayalakshmi, A. Morri, F. Rotundo, S. Toschi, R.A. Singh, Aluminum and Magnesium Metal Matrix Nanocomposites, Springer Singapore, Singapore, 2017. doi:10.1007/978-981-10-2681-2.

[7] J. Hashim, L. Looney, M.S.J. Hashmi, Metal matrix composites: production by the stir casting method, J. Mater. Process. Technol. 92–93 (1999) 1–7. doi:10.1016/S0924-0136(99)00118-1.

[8] H. Choi, J. Shin, B. Min, J. Park, D. Bae, Reinforcing effects of carbon nanotubes in structural aluminum matrix nanocomposites, J. Mater. Res. 24 (2009) 2610–2616. doi:10.1557/jmr.2009.0318.

[9] M. Penchal Reddy, V. Manakari, G. Parande, F. Ubaid, R.A. Shakoor, A.M.A. Mohamed, M. Gupta, Enhancing compressive, tensile, thermal and damping

response of pure Al using BN nanoparticles, J. Alloys Compd. 762 (2018) 398–408. doi:10.1016/j.jallcom.2018.05.205.

[10] K.L. Firestein, S. Corthay, A.E. Steinman, A.T. Matveev, A.M. Kovalskii, I. V. Sukhorukova, D. Golberg, D. V. Shtansky, High-strength aluminum-based composites reinforced with BN, AlB2and AlN particles fabricated via reactive spark plasma sintering of Al-BN powder mixtures, Mater. Sci. Eng. A. 681 (2017) 1–9. doi:10.1016/j.msea.2016.11.011.

[11] Y.B. Liu, S.C. Lim, L. Lu, M.O. Lai, Recent development in the fabrication of metal matrix-particulate composites using powder metallurgy techniques, J. Mater. Sci. 29 (1994) 1999–2007. doi:10.1007/BF01154673.

[12] M.M. Castro, P.H.R. Pereira, A. Isaac, R.B. Figueiredo, T.G. Langdon, Development of a magnesium-alumina composite through cold consolidation of machining chips by high-pressure torsion, J. Alloys Compd. 780 (2019) 422–427. doi:10.1016/j.jallcom.2018.11.357.

[13] I. V. Alexandrov, Y.T. Zhu, T.C. Lowe, R.K. Islamgaliev, R.Z. Valiev, Consolidation of nanometer sized powders using severe plastic torsional straining, Nanostructured Mater. 10 (1998) 45–54. doi:10.1016/S0965-9773(98)00026-9.

[14] Y. Li, Z. Zhang, R. Vogt, J.M. Schoenung, E.J. Lavernia, Boundaries and interfaces in ultrafine grain composites, Acta Mater. 59 (2011) 7206–7218. doi:10.1016/j.actamat.2011.08.005.

[15] N. Chawla, K.K. Chawla, Metal Matrix Composites, Springer New York, New York, NY, 2013. doi:10.1007/978-1-4614-9548-2.

[16] J. Guo, J.M. Rosalie, R. Pippan, Z. Zhang, Revealing the Microstructural evolution in Cu-Cr nanocrystalline alloys during high pressure torsion, Mater. Sci. Eng. A. 695 (2017) 350–359. doi:10.1016/j.msea.2017.04.034.

[17] M. Ashida, Z. Horita, T. Kita, A. Kato, Production of Al/Al2O3 Nanocomposites through Consolidation by High-Pressure Torsion, Mater. Trans. 53 (2012) 13–16.

[18] A.P. Zhilyaev, T.G. Langdon, Using high-pressure torsion for metal processing: Fundamentals and applications, Prog. Mater. Sci. (2008). doi:10.1016/j.pmatsci.2008.03.002.

[19] H. Asgharzadeh, H.S. Kim, Microstructure and Mechanical Properties of Al-3 Vol% CNT Nanocomposites Processed by High-Pressure Torsion, Arch. Metall. Mater. 62 (2017) 1109–1112. doi:10.1515/amm-2017-0161.

[20] X. Sauvage, F. Wetscher, P. Pareige, Mechanical alloying of Cu and Fe induced by severe plastic deformation of a Cu-Fe composite, Acta Mater. 53 (2005) 2127–2135. doi:10.1016/j.actamat.2005.01.024.

[21] N. Khobragade, K. Sikdar, B. Kumar, S. Bera, D. Roy, Mechanical and electrical properties of copper-graphene nanocomposite fabricated by high pressure torsion, J. Alloys Compd. 776 (2019) 123–132. doi:10.1016/j.jallcom.2018.10.139.

[22] K. Edalati, S. Toh, H. Iwaoka, Z. Horita, Microstructural characteristics of tungsten-base nanocomposites produced from micropowders by high-pressure torsion, Acta Mater. 60 (2012) 3885–3893. doi:10.1016/j.actamat.2012.02.048.

[23] W.T. Sun, X.G. Qiao, M.Y. Zheng, C. Xu, S. Kamado, X.J. Zhao, H.W. Chen, N. Gao, M.J. Starink, Altered ageing behaviour of a nanostructured Mg-8.2Gd-3.8Y-1.0Zn-0.4Zr alloy processed by high pressure torsion, Acta Mater. 151 (2018) 260–270. doi:10.1016/j.actamat.2018.04.003.

[24] P. V. Liddicoat, X.Z. Liao, Y. Zhao, Y. Zhu, M.Y. Murashkin, E.J. Lavernia, R.Z. Valiev, S.P. Ringer, Nanostructural hierarchy increases the strength of aluminium alloys, Nat. Commun. 1 (2010). doi:10.1038/ncomms1062.

[25] R.B. Figueiredo, P.R. Cetlin, T.G. Langdon, Using finite element modeling to examine the flow processes in quasi-constrained high-pressure torsion, Mater. Sci. Eng. A528 (2011) 8198–8204.

[26] T. Tokunaga, K. Kaneko, K. Sato, Z. Horita, Microstructure and mechanical properties of aluminum–fullerene composite fabricated by high pressure torsion, Scr. Mater. 58 (2008) 735–738. doi:10.1016/J.SCRIPTAMAT.2007.12.010.

[27] Y. Huang, P. Bazarnik, D. Wan, D. Luo, P.H.R. Pereira, M. Lewandowska, J. Yao, B.E. Hayden, T.G. Langdon, The fabrication of graphene-reinforced Al-based nanocomposites using high-pressure torsion, Acta Mater. 164 (2019) 499–511. doi:10.1016/J.ACTAMAT.2018.10.060.

[28] K. Edalati, M. Ashida, Z. Horita, T. Matsui, H. Kato, Wear resistance and tribological features of pure aluminum and Al–Al2O3 composites consolidated

by high-pressure torsion, Wear. 310 (2014) 83–89. doi:10.1016/J.WEAR.2013.12.022.

[29] R. Ishikawa, A.R. Lupini, S.D. Findlay, T. Taniguchi, S.J. Pennycook, Three-dimensional location of a single dopant with atomic precision by aberration-corrected scanning transmission electron microscopy, Nano Lett. 14 (2014) 1903–1908. doi:10.1021/nl500564b.

[30] J. Hwang, J.Y. Zhang, A.J. D'Alfonso, L.J. Allen, S. Stemmer, Three-dimensional imaging of individual dopant atoms in SrTiO3, Phys. Rev. Lett. 111 (2013). doi:10.1103/PhysRevLett.111.266101.

[31] M. Bar-Sadan, J. Barthel, H. Shtrikman, L. Houben, Direct imaging of single Au atoms within GaAs nanowires, Nano Lett. 12 (2012) 2352–2356. doi:10.1021/nl300314k.

[32] A.S.M. Handbook, Alloy Phase Diagram, vol. 3, ASM, Mater. Park. OH. (1992) 426–427. doi:10.1007/BF02869318.

[33] G. Slama, A. Vignes, Diffusion dans les aluminiures de niobium, J. Less-Common Met. 29 (1972) 189–202. doi:10.1016/0022-5088(72)90190-7.

[34] F.R. De Boer, R. Boom, W.C.M. Mattens, A.R. Miedema, A.K. Niessen, Cohesion in Metals, 1988.

[35] C.P. De Lazzari, D.G. Simões, J.D.T. Capocchi, Study of the aluminothermic reduction of niobium pentoxide through thermal analysis experiments and high energy milling processing, Mater. Res. 10 (2007) 215–218. doi:10.1590/S1516-14392007000200020.

[36] K. Edalati, S. Toh, M. Watanabe, Z. Horita, In situ production of bulk intermetallic-based nanocomposites and nanostructured intermetallics by high-pressure torsion, Scr. Mater. 66 (2012) 386–389. doi:10.1016/J.SCRIPTAMAT.2011.11.039.

[37] S. V. Divinski, G. Reglitz, H. Rösner, Y. Estrin, G. Wilde, Ultra-fast diffusion channels in pure Ni severely deformed by equal-channel angular pressing, Acta Mater. 59 (2011) 1974–1985. doi:10.1016/j.actamat.2010.11.063.

[38] E.O. Hall, The deformation and ageing of mild steel: III Discussion of results, Proc. Phys. Soc. Sect. B. (1951). doi:10.1088/0370-1301/64/9/303.

[39] N.J. Petch, The cleavage strength of polycrystals, J. Iron Steel Inst. (1953). doi:10.1007/BF01972547.

[40] F.X. Li, P.D. Hao, J.H. Yi, Z. Chen, K.G. Prashanth, T. Maity, J. Eckert, Microstructure and strength of nano-/ultrafine-grained carbon nanotube-reinforced titanium composites processed by high-pressure torsion, Mater. Sci. Eng. A. 722 (2018) 122–128. doi:10.1016/j.msea.2018.03.007.

[41] J.F. Nie, Effects of precipitate shape and orientation on dispersion strengthening in magnesium alloys, Scr. Mater. 48 (2003) 1009–1015. doi:10.1016/S1359-6462(02)00497-9.

[42] A.J. Detor, C.A. Schuh, Grain boundary segregation, chemical ordering and stability of nanocrystalline alloys: Atomistic computer simulations in the Ni-W system, Acta Mater. 55 (2007) 4221–4232. doi:10.1016/j.actamat.2007.03.024.

[43] M. Legros, D.S. Gianola, K.J. Hemker, In situ TEM observations of fast grain-boundary motion in stressed nanocrystalline aluminum films, Acta Mater. 56 (2008) 3380–3393. doi:10.1016/j.actamat.2008.03.032.

[44] D.L. Medlin, K.F. McCarty, R.Q. Hwang, S.E. Guthrie, M.I. Baskes, Orientation relationships in heteroepitaxial aluminum films on sapphire, Thin Solid Films. 299 (1997) 110–114. doi:10.1016/S0040-6090(96)09393-5.

[45] G. Pilania, B.J. Thijsse, R.G. Hoagland, I. LaziÄ, S.M. Valone, X.Y. Liu, Revisiting the Al/Al 2 O 3 interface: Coherent interfaces and misfit accommodation, Sci. Rep. 4 (2014). doi:10.1038/srep04485.

[46] X. Zhang, S. Li, B. Pan, D. Pan, S. Zhou, S. Yang, L. Jia, K. Kondoh, A novel strengthening effect of in-situ nano Al2O3w on CNTs reinforced aluminum matrix nanocomposites and the matched strengthening mechanisms, J. Alloys Compd. 764 (2018) 279–288. doi:10.1016/j.jallcom.2018.06.006.

[47] B. Chen, S. Li, H. Imai, L. Jia, J. Umeda, M. Takahashi, K. Kondoh, Carbon nanotube induced microstructural characteristics in powder metallurgy Al matrix composites and their effects on mechanical and conductive properties, J. Alloys Compd. 651 (2015) 608–615. doi:10.1016/j.jallcom.2015.08.178.